LAWRENCE
LIVERMORE
NATIONAL
LABORATORY

UCRL-JRNL-204838-REV-1

Intelligent Signal Processing for Detection System Optimization

C. Y. Fu, L. I. Petrich, P. F. Daley, A. K. Burnham

December 13, 2004

Analytical Chemistry

Intelligent Signal Processing for Detection System Optimization

Chi Yung Fu,*[†] Loren I. Petrich,[‡] Paul F. Daley[†] Alan K. Burnham[†]

[†]***Lawrence Livermore National Laboratory, Livermore, CA 94550***

[‡]***University of California, Berkeley, CA 94720***

A wavelet-neural network signal processing method has demonstrated approximately tenfold improvement over traditional signal-processing methods for the detection limit of various nitrogen and phosphorus compounds from the output of a thermionic detector attached to a gas chromatograph. A blind test was conducted to validate the lower detection limit. All fourteen of the compound spikes were detected when above the estimated threshold, including all three within a factor of two above the threshold. In addition, two of six spikes were detected at levels of 1/2 the concentration of the nominal threshold. Another two of the six would have been detected correctly if we had allowed human intervention to examine the processed data. One apparent false positive in five nulls was traced to a solvent impurity, whose presence was subsequently identified by analyzing a solvent aliquot evaporated to 1% residual volume, while the other four nulls were properly classified. We view this signal processing method as broadly applicable in analytical chemistry, and we advocate that advanced signal processing methods should be applied as directly as possible to the raw detector output so that less discriminating preprocessing and post-processing does not throw away valuable signal.

*E-mail: fu1@llnl.gov

Progress in analytical chemistry over the years has enabled increasingly lower detection limits. Much of this has been due to advances in electronics, better materials, and better microfabrication capabilities. One area that does not appear to have been fully exploited yet is advanced signal processing, which can be a key component of any sensing system. If not done well, the preprocessing inherent in any instrument design can throw away valuable information, and subsequent use of advanced signal processing methods, no matter how capable, will not be able to recover signal lost by crude pre-processing. A very significant advantage in utilizing advanced signal processing is that as more capable algorithms are available, upgrading system performance can be very simple, because it entails no hardware component changes and no expensive systems to replace.

It is useful at the outset to contrast the objective of our work to other signal interpretation activities. Chemometrics[1] ordinarily looks at methods of separating a signal into its constituent parts, be it determining the relative fractions of spectral mixtures, as in principal component analysis, or resolving overlapping spectral or chromatographic peaks. Instead, the focus here is to separate the signal from noise coming from instrumentation and/or the detector so that it is more amenable to interpretation by chemometrics or other methods. Two recent review articles[2,3] report only a few papers on denoising. One can conceive of hybrid systems in which the integration of separation from noise and separation into components maximizes system performance.

Combination of multiple signal processing methods has the potential to extract information more completely than by using a single method. Different non-redundant methods have different strengths and weaknesses, and appropriate combinations can take advantage of these different characteristics. Biological systems, such as vision, often use such combinations.[4]

We have developed an intelligent signal processing method that can be a central aspect of optimized system design and extraction. It is based on an adaptive combination of wavelet filtering and neural network processing. Because our system was inspired by biological systems, we call it BISP, which stands for biological inspired signal processing. It is currently implemented with a graphical user interface to enable various users to access these advanced techniques. In the long term, this type of method could be built into a signal-processing chip (ASIC, full-custom, or DSP) for real time processing, especially when handling the enormous amount of data that some 2-D or 3-D high-resolution sensors collect.

In this work, we show that it is possible to reliably extract gas chromatographic (GC) peaks at signal-to-noise levels substantially less than one. This method has demonstrated at least a tenfold improvement over more conventional methods based on running averages and a low-pass analog filter. We view this demonstration as prototypical of what might be possible for a wide range of analytical detection devices.

MATHEMATICAL METHODS

The entire signal extraction process can be summarized by the following sequence of operations: (a) removing background or other long-scale-length variations through spline-fitting, (b) wavelet decomposition and/or denoising of each of the wavelet components, (c) using separate neural networks for signal extraction working in the wavelet domain for each unprocessed or processed wavelet component, (d) combining the outputs of all the neural networks, and finally (e) applying an inverse wavelet transform to return a clean signal in the time domain. This is shown schematically in Figure 1 and is explained in detail in this section.

Wavelets are a kind of transform that break data into coefficients in both time and frequency, thus getting around a major difficulty of the Fourier transform, which lose all time information during the transform. Many sorts of data have important features that are localized in time, etc., like spectra, gas-chromatography readouts, etc., and applying a wavelet transform will preserve this time localization. Preserving exact peak locations while denoising is a very important constraint on signal processing for methods such as gas chromatography.

A Fourier transform works by finding a set of coefficients for different-frequency sine waves, which, when added together, will reproduce the original data. Because these sine waves stretch over the entire time of the transform, the loss of time information is readily understandable. By comparison, a wavelet transform works by finding a set of coefficients for wavelet functions, which when added together, will produce the original data. These wavelet functions are actually a single localized function that has been shifted and stretched in time by various amounts to provide a set of basis functions to synthesize the signal. The shifting captures time information, while the stretching captures frequency information (the frequency is the reciprocal of the amount of stretch). These compact localized basis functions of the wavelet approach enable the wavelet transform to maintain simultaneous time and space (or frequency) information, a very important difference from the Fourier transform.

Such fitting seems like a difficult task, but there is a convenient shortcut algorithm for doing the fitting in the discrete case. One applies a pair of wavelet filters to the original data and keeps every second point of both, thus retaining the original number of data points. These filters may be described as smooth (finds the average) and rough (finds the details). The smooth part is approximately a local average of the data, while the rough part contains the local details.

This operation can be repeated on the resulting smooth part, resulting in a new smooth part and a rough part corresponding to a length scale twice as large as the original's. Continuing this process repetitively produces a sequence of rough parts for length scales increasing as 1, 2, 4, 8, … (powers of 2), with a smooth part at the highest length scale. The length scales correspond to frequencies 1, 1/2, 1/4, 1/8, … as one goes up the sequence, and the indices of data points in a particular part correspond to time, with neighboring data points being separated in time by 1, 2, 4, 8, … as one goes up the sequence.

This operation can be undone with a similar sort of filtering, which is especially convenient if one wishes to proceed with further processing of the data in its untransformed form. And with appropriate selection of filters, the forward and inverse filters can be made identical. Such "orthogonal" filters include the Daubechies and Coifman filter families.

Our wavelet preprocessing, or more precisely, discrete wavelet transform (DWT), serves three different purposes. First, it provides a means to segment the data in a way that enables time-saving progressive processing. The specific method used for this work is a 4-level decimated Daubechies-2 wavelet transform,[5,6] which has a shape similar to the Gaussian with exponential tail characteristic of GC peaks. Second, signals most often occur within the smoother scales, which were decimated repeatedly by the DWT process. Consequently, such decomposition allows us to automatically achieve data reduction if using such smoother components proves to be sufficient, as it is in this case here. A 16-fold data reduction was accomplished in this work. Third, the smoothness of the lower scales allows neural networks to perform better in those wavelet component domains. In other words, the transform provides a way to "transfigure" the data into a domain that favors neural network processing.

The function of the neural network[7,8] is to extract relevant features that it learns from the training process. The training tunes the neural network to recognize certain common features that would occur in the targeted signals. A unique feature of our neural network processing is that data is processed in the wavelet domain to take advantage of both smoothness of the signals and the data reduction in the smoother scales. Secondly, by using or allowing more than one neural network, we have devised a divide-and-conquer technique. Separate neural networks may handle separate decomposed wavelet signals representing different scales. Together, we have a progressive system that allows us to trade off computational complexity with accuracy. Furthermore, because of the adaptiveness of neural networks, we do not have to precisely tune the wavelet preprocessing for absolute optimal denoising. The two systems overlap and thus yield a more flexible or "forgiving" signal processing.

The specific approach we use is a projection neural network. Artificial neural networks mimic their biological counterparts by using networks of interconnected neurons through appropriate synaptic connections to perform simple but effective parallel computations. A neuron can be a simple "fire or not-fire" processing element or, more effectively, a computation unit that sums all its inputs modified by the corresponding synaptic strengths as defined by the synaptic values; then the summation is further modified by a non-linear transfer function. A projection neural network projects the original input vectors into a space with one higher dimension before feeding the projected vectors into a single-hidden-layer feed-forward backpropagation neural network. A modified Logicon projection system is used for this processing, which, as shown schematically in Figure 2, enables the hidden unit's decision boundaries to take on a much greater variety of shapes, such as an ellipse, compared to straight lines in the case of backpropagation neural network.[9] Also, we use vector quantization to determine initial conditions for more efficient

training. Together, these lead to more efficient use of neurons—we typically need only 6 or 9 neurons, which enables fast and efficient generalization. Because of the four orders of magnitude change in the dynamic range of the input data, we used four different neural networks to handle the different ranges, and each of these four neural networks use either 6 or 9 neurons. The projection is described mathematically by

$$I'_k = S\frac{(I_k / R)}{1+\sum_m (I_m /(2R))^2} \tag{1a}$$

and

$$I'_{extra} = S\frac{1-\sum_m (I_m /(2R))^2}{1+\sum_m (I_m /(2R))^2} \tag{1b}$$

where I'_k is the projected input based on I_k; I'_{extra} is the extra projected input to raise the dimension by one; R is the projection radius; and S is the projection size.

Data is projected according to these equations, and vector quantization is performed to obtain an initial weight vector for each hidden neuron. The projection creates a new input dataset one dimension higher than the original dataset because of the I'_{extra}. The projected input data are initially assigned randomly to the hidden units, and quantization is done by iteration using the Linde-Buzo-Gray algorithm.[10] This new dataset is then fed into a feed-forward neural network for training. Many different training algorithms can be used, including conventional gradient descent, quasi-Newton, and conjugate gradient methods.[11]

EXPERIMENTAL SECTION

The target analytes used in this study were chosen from a set of surrogate compounds proposed for characterizing instruments for detection of chemical weapons, and they included organophosphates, pesticides, and nitrogen containing materials. Specific compounds used were trimethylphosphate (TMP), 99+%; tributylphosphate (TBP), 99+%; 1-fluoro-4-nitrobenzene (FNB), 99%; and 5-chloro-2-methylaniline (CMA), 97% (Aldrich, Inc.); Malathion (Mal, [(dimethoxyphosphino-thioyl)thio]butanedioic acid diethyl ester), 98.2% (Chem Service, Inc., West Chester, PA); and Amiton (Am, S-[2-(diethylamino)ethyl]phosphoro-thioic acid O,O-diethylester), 98% (Edgewood Aresenal). Compounds were dissolved in dichloromethane (Mallinckrodt SpectrAR®, 99.5% min.), and dilutions were prepared using volumetric ware and gastight analytical syringes. Solutions were sealed in septum-capped vials for use, and septa were replaced at the end of each day to prevent solvent loss. All materials were used without further purification.

Compounds were separated on an HP/Agilent 5890 GC equipped with a capillary column (DB-5, 10m x 0.100 mm, 0.10µ film, J&W Scientific). The carrier was helium. The column head pressure of 50 psi gave a flow rate of approximately 0.5 $ml \cdot min^{-1}$. Liquid injections (1.0 µl throughout) were made with the split-splitless injector held at 250 °C, operated in the splitless mode with a 2 mm, silanized, straight-bore injection sleeve (Supelco, Inc.) and a purge "off" time of 30 s following injections. Optimum precision was achieved using a hot needle technique (Grob, 2001), with a preinjection heating period of five seconds. Split vent and septum purge flows were maintained at 10.0 and 1.0 $ml \cdot min^{-1}$, respectively. The column oven was time-

temperature programmed: 40 °C, 20 s hold, 50 °C·min^{-1} to 200 °C, then 30 °C·min^{-1} to 270 °C, with a 1 min final hold. All target compounds were eluted within six minutes (Figure 3).

Compound elution times were confirmed with detection by an HP/Agilent 5970 mass selective detector, and comparison of spectra with NIST libraries, prior to attaching the column to a thermionic detector (Detector Engineering & Technology, Inc., Walnut Creek, CA), equipped with TID-2 detector beads, operated in the N-P mode with air/H_2 makeup gas (50.0 and 2.4 ml·min^{-1}, respectively), and held at 300 °C. Beads were exchanged when baseline depression following the solvent peak became significant; generally this was within five to seven days of installation. We observed that even though the thermionic detector maintained good sensitivity, there was subtle drift in response. To minimize this effect, particularly during collection of data for "blind" processing with the combined signal processing approach, filtered and unfiltered runs were interleaved for each sample; samples were analyzed in triplicate with unfiltered signal capture, and in duplicate for filtered capture. Similarly, "blind" mixtures and known standard blends were interleaved.

As we intended to evaluate the utility of the combined signal processing approach to enhance sensitivity for medium-resolution, portable analytical equipment, we captured chromatograms with a 12-bit analog to digital PCMCIA card (DAQ-Card 1200, National Instruments, Inc. Austin, TX), using in-house, custom LabVIEW programs for signal acquisition. Signals were designated as either "filtered" (10 Hz low-pass, two-pole R-C filter; sampling at 200 Hz, 50-point software moving average), or "unfiltered" (no R-C filtering, sampling at 1000 Hz, 3-point software moving average). Filtered data were analyzed with a custom LabVIEW chromatogram analyzer, based on peak detection from first derivatives calculated on moving

eight point data windows; unfiltered data could not be analyzed with this software, and they were processed separately with the combined wavelet/neural network system.

RESULTS AND DISCUSSION

Figure 4 shows the kind of signal recovery that can be attained using the combined wavelet-neural network method. Repeated measurements recover the signal from two nitrogen compounds having a signal-to-noise of ~0.16, where the noise is the full peak-to-valley width. Even though the peaks are only twice as large as the bit resolution of the A/D converter**,** they are recovered cleanly, suggesting that the detection limit is considerably lower. When used separately, neural networks performed better than wavelets, but neither performed as well as the combination.

An obvious question is how well this method compares to other methods. Much of the noise is high frequency, so a simple multiple-point running average can improve the signal-to-noise ratio several fold, although peak broadening is produced by this approach and thus may affect the exact peak positions. Even more noise reduction can be achieved with more sophisticated filtering. We chose a Butterworth/matched filters combination for comparison. A Butterworth filter has a smooth response and relatively gentle rolloff compared to other filters, such as the Chebyshev filter, and our parameter settings were chosen so the Butterworth filter acted as a lowpass filter. A comparison of signal recovery using the Butterworth/matched filtering and the wavelet-neural network method is shown in Figure 5. Although the four peaks were resolved by the Butterworth/matched filters combination, the doublets of the two peaks at ~5000 and ~12500 were not resolved by it, even though they were made visible using BISP. In

addition, the poor noise floor from the Butterworth/matched filters would lead to false peak detection.

A test matrix was constructed to determine the factor of improvement in detection sensitivity and the reliability of detection using the wavelet-neural network signal processing algorithms. The first part of the test matrix consisted of seven calibration solutions having a 200-500 fold range in concentration of each of the target compounds. The lowest concentration turned out to be lower than the detection limit ultimately achieved by BISP based on our current height threshold for detection, and one intermediate-concentration solution was rejected from regression as statistical outlier, likely a result of detector drift. Consequently, the calibration was based on five solutions. The second part consisted of 5 blind samples having various concentrations of the calibrated compounds, with some nulls, and two spikes of a blind compound (Amiton) near its suspected detection limit. The complete comparison process is shown for one sample near the detection limit in Figure 6.

A typical calibration curve is shown in Figure 7 to illustrate two points. At high concentrations, variations in injection and detector performance limit the precision of the peak areas to a range of 2-3. Near the detection limit, the integrated peak area can vary by more like a factor of ten. Additional details are given in the supplemental material. Detection limits for the wavelet-neural network method, based on current threshold setting for peak identification, were approximately 1 pg for Malathion and the two alkyl phosphates, 10 pg for chloromethylanaline, and 30 pg for fluoronitrobenzene. The detection limit for the conventional data processing was 10 to 50 times larger when compared at the same level of human intervention—automatic peak detection using mathematical criteria. Peaks are visible at 2-3 times lower concentration, but they are not reliably above false peaks due to noise. Even lower detection limits for BISP are possible

by lowering the threshold setting; however, more sensitive detection will result in more false detections. The tradeoff between sensitivity and false positives is typically characterized by a ROC curve, but we did not do that extensive of a characterization. At this detection threshold, about 10 “extraneous” peaks were detected, but most were later attributed to reproducible impurities. After eliminating known impurities, BISP has 3.5 unassignable, and likely false, peaks over the entire chromatogram (not within target molecule retention-time windows), while conventional processing using the same detection threshold yields over 200 extraneous, and likely false, peaks. As a result, BISP can be made much more sensitive before its false detection level matches that of conventional processing.

The results of the blind test are given in Table 1, which includes the formulated and measured concentrations. The ratios of measured-to-formulated concentrations vary similarly in magnitude to replicate runs in the calibration data in Figure 7. All spikes greater than the nominal detection threshold were detected, albeit sometimes with a relatively large error consistent with the large deviation in the calibration area near the threshold. In one null case, a small peak was reported. Subsequent inspection showed that this was due to a solvent impurity, which introduces the double blind aspect of the test.

During the calibration process, up to twelve small extraneous peaks not associated with the known spiked compounds were observed frequently, but not always, in the gas chromatograms. An obvious explanation is that these might be impurities in the solutions that are not above signal to noise using conventional methods but were extracted using BISP. This explanation was verified by evaporating a portion of solvent to 1% residual volume and injecting the concentrate into the gas chromatograph. About half the extraneous peaks were present in the solvent concentrate (examples in the supplementary material). Because the levels are so low, it

is possibly that many of the others were picked up during solution handling and processing. Consequently, the true false positive rate, though difficult to estimate quantitatively, is very low.

One additional aspect of the blind test was the addition of Amiton at the 0.5 and 1.5 pg levels, respectively, in two of the solutions. This material was not part of the calibration set and was unknown to those doing the wavelet-neural net signal processing. Even so, the 0.5 pg spike was detected in three of three injections and reported as an unknown hit. The 1.5 pg was detected in two of three injections, but it was not initially reported as a reliable hit, because we typically set the criteria for detection as 4 detections out of 6 trials (two neural nets operating on three injectuions). These variations in detection certainty are consistent with the considerable variation in quantified area near the detection limit.

We believe that this is the first reported work using a combination of wavelet and artificial neural network technologies to extract trace peaks found in chromatography. Other researchers have applied neural network technology in this area, but most of the twenty-three citations we found are not relevant to the work reported here. There are two citations for using both wavelet transforms and artificial neural networks on chromatography, but the objective was classification, not trace signal extraction, and the mathematical details are significantly different.

Voisin[12] and Hernandez-Borges[13] reported processing the spectra by neural networks to identify bacteria based on certain identifiers such as the concentration of n-alkanes or fatty acids as measured by gas chromatography. Fatemi[14] and Jalali-Heravi[15] reported using ANN's to learn from certain chemical parameters such as molecular weights and energy levels of the highest occupied molecular orbitals, to predict retention indices or retention time, whereas Bell[16] and Cai[17] reported using the spectra as inputs to the neural network for chemical classification such as level of toxicity or active substructures. Our work is more fundamental. We report here using

neural networks to recognize components of the spectra— either part of a peak or the entire peak. We use a moving window to keep the size within reasonable limits, whereas previous reported work[12,13,16,17] used the full spectrum. Each pass through our neural network yields a single point on the spectrum, whereas the outputs of others' neural networks yield different classifications. As a result, our work dovetails with these reported works, because if the spectra can be made clean and noise-free, then classification can be done relatively easily.

The two references using both wavelet and neural network on chromatography are for liquid chromatography. Collantes[18] reported using wavelets and neural networks on HPLC data for the classification of L-tryptophan from six different manufacturers. Similar to the work here, they used wavelet preprocessing, but the details are very different. They used a wavelet package (a combination of wavelets and an oscillating function), whereas we use pure wavelets. Use of the Haar function does not have a clear justification, since the stepwise function of Haar function makes it ill suited for extracting smooth data, which is our goal. However, for the purpose of classification into the six different manufacturers, details may not be needed, and Haar wavelets do offer computation simplicity. Probably for the same reason, they only retained some of the most important, but not all, wavelet coefficients as inputs to the neural network. However, these coefficients alone were not sufficient, so they were supplemented with their corresponding positional information. They used relatively straightforward backpropagation neural networks for the purpose of classification, and achieved good results. Much like the works cited in the previous paragraph, this work is mostly restricted to doing classification.

Schirm[19] reported using a combination of wavelet processing and neural network for quality assurance of pentosan polysulfate based on fingerprint electropherograms. They reported using Coiflet wavelets, which have higher computational demand than Haar or Dachechies-2

wavelets, to preprocess the electrophoresis data. They found that using a combination of mid-level transforms yields the best results for baseline and noise considerations, whereas we simply use the smoothest level and have shown that it retains all vital information for our peak reconstruction. The best approach to wavelet preprocessing probably depends on the type of data to be processed as well as the purpose of such preprocessing. Schirm's objective is to provide wavelet processed data as inputs to the neural network for the purpose of classification, whereas we are trying to use our neural network to extract trace peaks. Collantes, Schirm, and our work reported here indicate that the types and the details of preprocessing are important considerations for effective signal processing design especially under resources constraints. Schirm used a simple backpropagation neural network, which performs the classification well. Our experience with backpropagation is that it is inadequate for pulling out trace signals. Both Schirm and we share the same assessment that a complete optimization of all neural network parameters would be extremely time-consuming.

CONCLUSIONS

Advanced signal processing methods, as exemplified by the wavelet-neural network approach shown here, have the potential to extract signals for at least ten times lower signal to noise than standard filtering and averaging techniques. Although we have not done an exhaustive comparison of all conceivable methods, the wavelet-neural network approach is better than any other we have tried. The detection limit turned out to be lower than the bit resolution of the data acquisition equipment. Consequently, we were not able to truly determine the absolute sensitivity achievable with our BISP approach — it could be significantly more than a factor of ten better than a conventional approach.

Our method should be generally applicable to a variety of chemical analysis equipment. The current method, with proper calibration, works on any one-dimensional array, so spectra as well as chromatograms are treatable. Extensions to two-dimensional data (e.g., spectra versus time, as in GC/MS) are possible. The method really only accomplishes signal recovery, not signal interpretation, so it is different from the typical objectives of chemometrics. However, without signal recovery, chemometrics will not be able to achieve its objectives. As a result, the two methods are not redundant but complementary to each other. The enhanced signal recovery might be especially important in small portable devices, which seek to minimize power consumption at the expense of detection capability. For instruments that operate in the signal-averaging mode, it is important to remember that a tenfold difference in signal-to-noise detection limit translates into a hundredfold difference in signal acquisition time, because the signal-to-noise ratio increases as $t^{1/2}$.

ACKNOWLEDGMENT

This work was performed under the auspices of the U.S. Department of Energy by the University of California, Lawrence Livermore National Laboratory, under Contract W-7405-Eng-48. We thank the NA22 office of DOE, particularly Dr. Leslie Pitts, for its support.

REFERENCES

(1) Lavine, B. K.; Workman, J. Jr. *Anal. Chem.* **2002**, 74, 2763-2770.

(2) Lavine, B. K. *Anal. Chem.* **1998**, 70, 209R-228R.

(3) Marshall, J.; Chenery, S.; Evans, E. H.; Fisher, A. *J. Anal. Atom. Spec.* **1998**, 13, 107R-130R.

(4) Brigner, W. L. *Percept. Mot. Skills* **2003**, 97(2), 407-23.

(5) Kaiser, R. *A Friendly Guide to Wavelets*, Birkhäuser, Boston **1994.**

(6) Daubechies, I. *Ten Lectures on Wavelets, CBMS-NSF Lecture Notes nr. 61*, SIAM, **1992**.

(7) Lippmann, R. *ASSP Magazine, IEEE* [see also IEEE Signal Processing Magazine], **1987**, 4, 4-22.

(8) Rumelhart, D. E.; Hinton, G.E.; Williams, R.J. *Parallel Data Processing*, M.I.T. Press, Cambridge, **1986**.

(9) Wilensky, G.D.; Manukian, N. *IJCNN: International Joint Conference on Neural Networks*, **1992**, 2, 358 - 367.

(10) Wu, F.H.; Ganesan, K. *Acoustics, Speech, and Signal Processing*, **1989**, 2, 751 -754.

(11) Press W.; Vettering, W. T.; Teukolsky, S. A.; Flannery, B. P. *Numerical Recipes in C - The Art of Scientific Computing*, Cambridge University Press, **1992.**

(12) Voisin, S.; Terreux, R; Renaud, F. N.; Freney, J.; Domard, M; Deruaz, D. *Antonie Van Leeuwenhoek.* **2004**, 4, 287-96.

(13) Hernandez-Borges, J.; Corbella-Tena, R.; Rodriguez-Delgado, M. A.; Garcia-Montelongo, F. J.; Havel, J. *Chemosphere* **2004**, 8, 1059-69.

(14) Fatemi, M. H. *J. Chromatogr. A.* **2002**, 2, 273-80.

(15) Jalali-Heravi, M.; Garkani-Nejad, Z. *J. Chromatogr. A.* **2002**,1-2, 173-84.

(16) Bell, S.; Nazarov, E.; Wang, Y. F.; Eiceman, G. A. *Anal. Chim. Acta.* **1999**, 394, 121-33.

(17) Cai, C.; Harrington, P. B. *Anal. Chem.* **1999**,19, 4134-41.

(18) Collantes, E. R.; Duta, R.; Welsh, W. J.; Zielinski, W. L.; Brower, J. *Anal. Chem.* 69, 1392-7.

(19) Schirm, B.; Benend, H.; Watzig, H. *Electrophoresis* **2001** 22, 1150-62.

Table 1. Comparison of formulated and reported concentrations for the blind test.

Compound (approx. detection limit)		1	2	3	4	5
Trimethyl phosphate	injected	1.6	None	53	260	0.5
(1 pg)	*reported*	*2.2*	*n.d.**	*66*	*193*	*n.d.*
Tributyl phosphate	injected	1.6	268	0.5	54	none
(1 pg)	*reported*	*3.4*	*500*	*1.5*	*23*	*n.d.*
Malathion	injected	1.5	51	0.5	102	none
(1 pg)	*reported*	*7.7*	*58*	*2.6*	*47*	*(0.6)***
Chloro-methylaniline	injected	53	none	265	1060	5.3
(10 pg)	*reported*	*92*	*n.d.*	*415*	*417*	*d.*
Fluoro-nitrobenzene	injected	11.8	590	5900	5.9	none
(30 pg)	*reported*	*d.*	*750*	*9415*	*n.d.*	*n.d.*

**n.d.* = not detected

***actually due to a solvent impurity peak

****d.* = detected based on manual examination

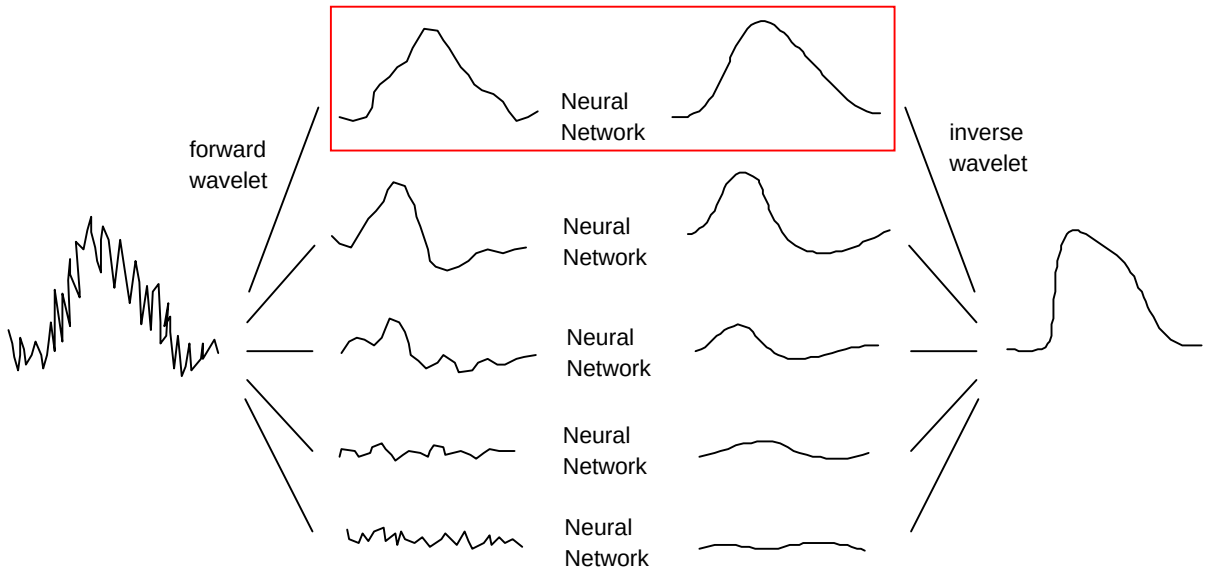

Figure 1. Procedure flow for wavelet/neural net processing. Incoming noisy data were first transformed and segmented by wavelet processing into different scales. Each component is then processed by its own neural network. The neural net outputs are then inversely transformed into the time domain. For the GC signals analyzed here, using the smoothest wavelet component contains most of the real signal sufficient, yielding a 16-fold reduction in the amount of the data for the neural network to learn.

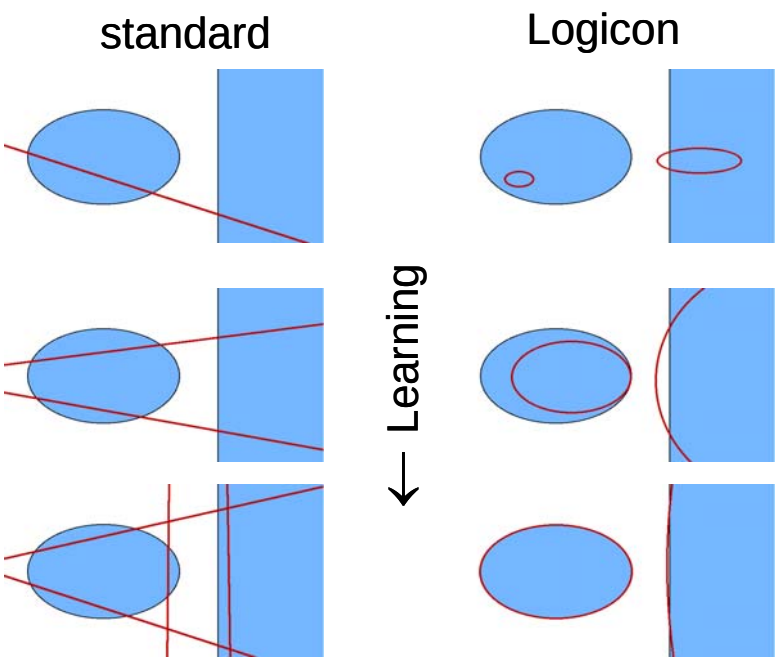

Figure 2. Schematic representation of the difference in how standard backpropagation and a Logicon projection neural network delineate segment boundaries. The higher dimensionality of the Logicon projection neural enables a better representation of nonlinear boundaries with fewer neurons and correspondingly fewer synaptic connections.

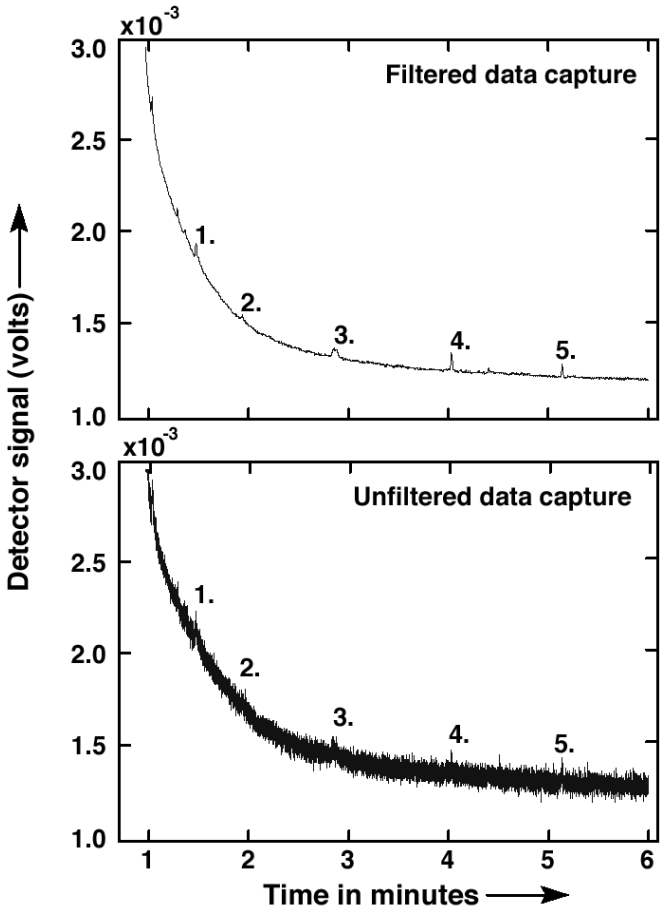

Figure 3. Sections from representative filtered (upper) and unfiltered (below) chromatograms. Peaks are: 1. TMP (5.3 pg), 2. FNB (59 pg), 3. CMA (53 pg), 4. TBP (5.3 pg) and 5. (Mal (5.1 pg). Amiton was not included in this run, but it eluted just after TBP.

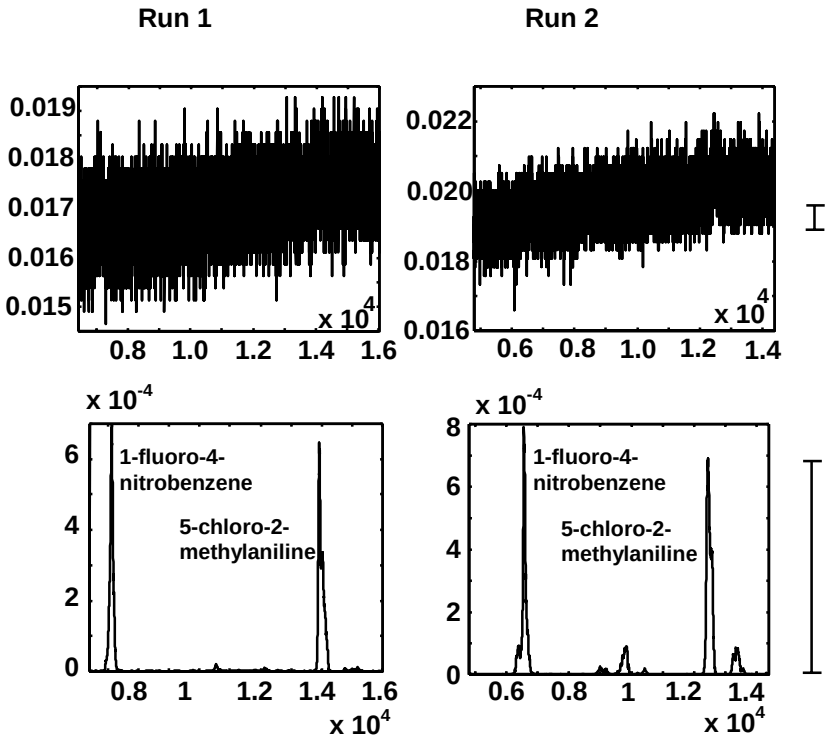

Figure 4. Replicate recoveries fluoronitrobenzene and chloromethylaniline peaks at very low levels in a gas chromatogram (abscissa is point number, not time). The small peaks may or may not be real. The two scale bars for Run 2 show the relative scales for the upper and lower figures.

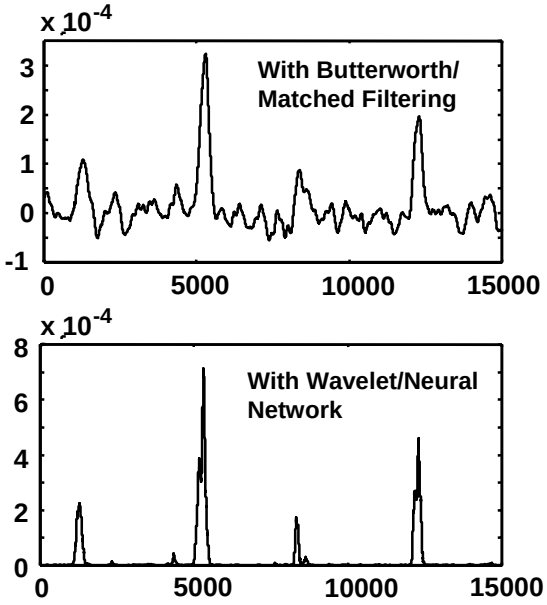

Figure 5. Comparison of recovered gas chromatographic peaks from noisy data (comparable to that in Fig. 1) using Butterworth/matched filtering and wavelet/neural net filtering.

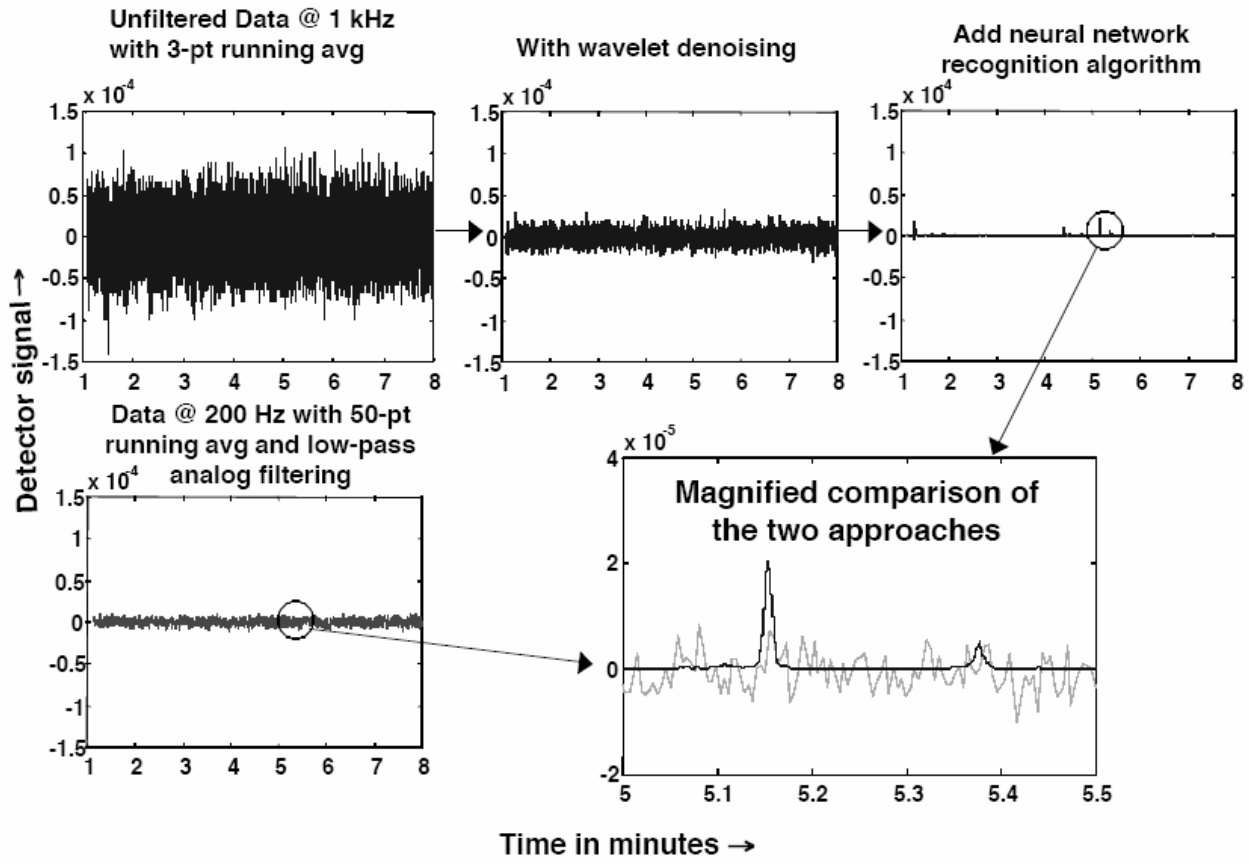

Figure 6. Comparison of the conventional (lower left) and BISP wavelet-neural network (upper right) methods of data processing. The expanded comparison in the lower right shows clearly the superiority of the advanced signal processing method for extracting low-level signals.

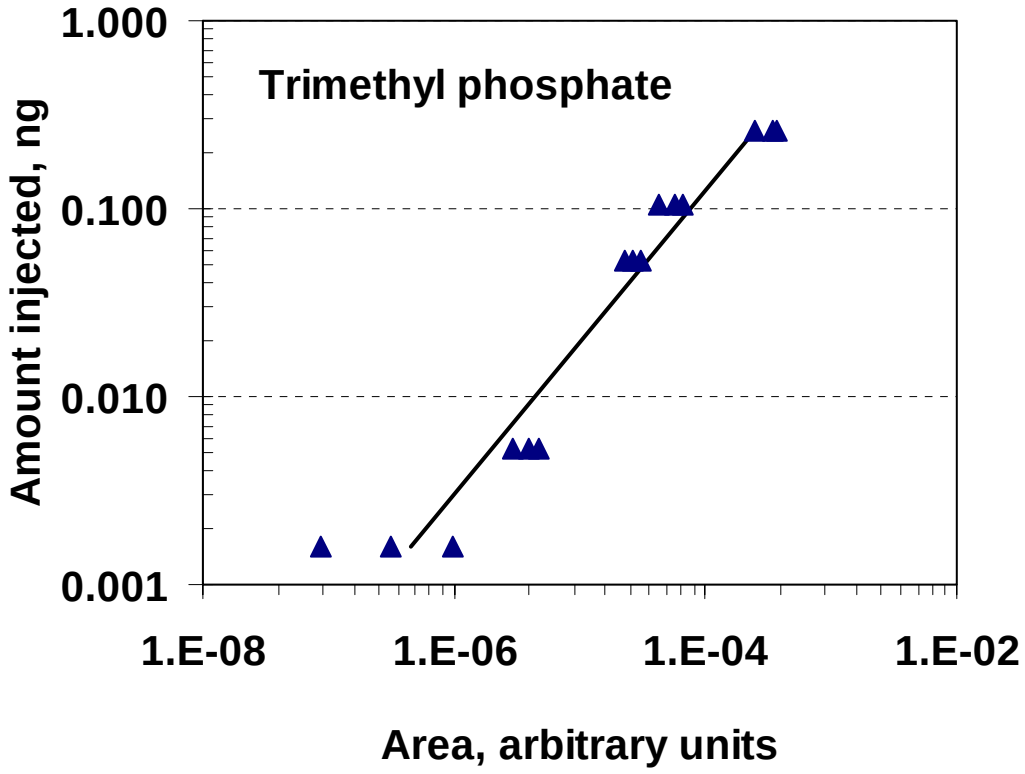

Figure 7. Typical calibration curve derived from the wavelet-neural network method. This is created in the "application" mode, i.e., the abscissa is a measured area used to calculate the corresponding amount present.

Supplemental Material

In the first step, a series of solutions were made to act as calibration standards for both the conventional and BISP method of data analysis. They were made by successive dilution. The properties of these calibration standards are given in Table S1. The concentrations of fluoronitrobenzene and chloromethylaniline are higher in order to achieve approximately the same detector area for compounds containing nitrogen rather than phosphorus.

Table S1. Concentrations in calibration solutions for five calibration compounds (ng/μl).

Compound	N	O	P	Q2	R	S	T
Trimethyl phosphate	0.263	0.105	0.0525	0.0158	0.00525	0.001575	0.000525
Tributyl phosphate	0.268	0.107	0.0535	0.0161	0.00535	0.001605	0.000535
Malathion	0.255	0.102	0.0510	0.0153	0.00510	0.00153	0.000510
1-Fluoro-4-nitrobenzene	5.90	1.18	0.590	0.118	0.05900	0.01180	0.00590
5-Chloro-2-methylaniline	1.060	0.530	0.265	0.106	0.05300	0.01060	0.00530

Detection limits for the conventional method of data collection and processing ("filtered data"= 10 Hz low-pass, two-pole R-C filter; sampling at 200 Hz, 50-point software moving average) were determined with a custom LabVIEW chromatogram analyzer, based on peak detection from first derivatives calculated on moving eight point data windows. Peak area results from an analysis of these calibration solutions are given in Table S2.

Table S2. Peak areas of "filtered data" from the calibration solutions in Table S1.

Compound	N	O	P	Q2	R
Trimethyl phosphate	18.57	2.64	2.07	0.18	n.d.
(TMP)	20.17	4.44	2.26	0.32	0.02
Tributyl phosphate	7.71	1.24	0.73	0.13	n.d.
(TBP)	6.65	1.90	0.84	n.d.	0.37
Malathion	8.07	1.25	0.91	0.13	0.24
(Mal)	8.87	1.94	1.00	0.12	0.09
1-Fluoro-4-nitrobenzene	23.13	0.38	0.41	n.d.	n.d.
(FNB)	29.02	0.71	0.49	n.d.	n.d.
5-Chloro-2-methylaniline	11.42	1.01	0.52	n.d.	0.22
(CMA)	14.87	1.53	0.55	0.07	n.d.

Plots of area versus amount injected (ng in 1 μl), shown in Figure S1, were used to assess the (reliable) detection level by LabVIEW using filtered data. Qualitatively, this corresponds to two of two analyses giving the same area within a factor of two. Formally, the detection level would depend on the required confidence level, but our data are too sparse to warrant a more rigorous statistical analysis, and our detection limits are accurate to a factor of two or three. Similar plots are shown in Figure S2 for the wavelet/neural network processing of filtered data.

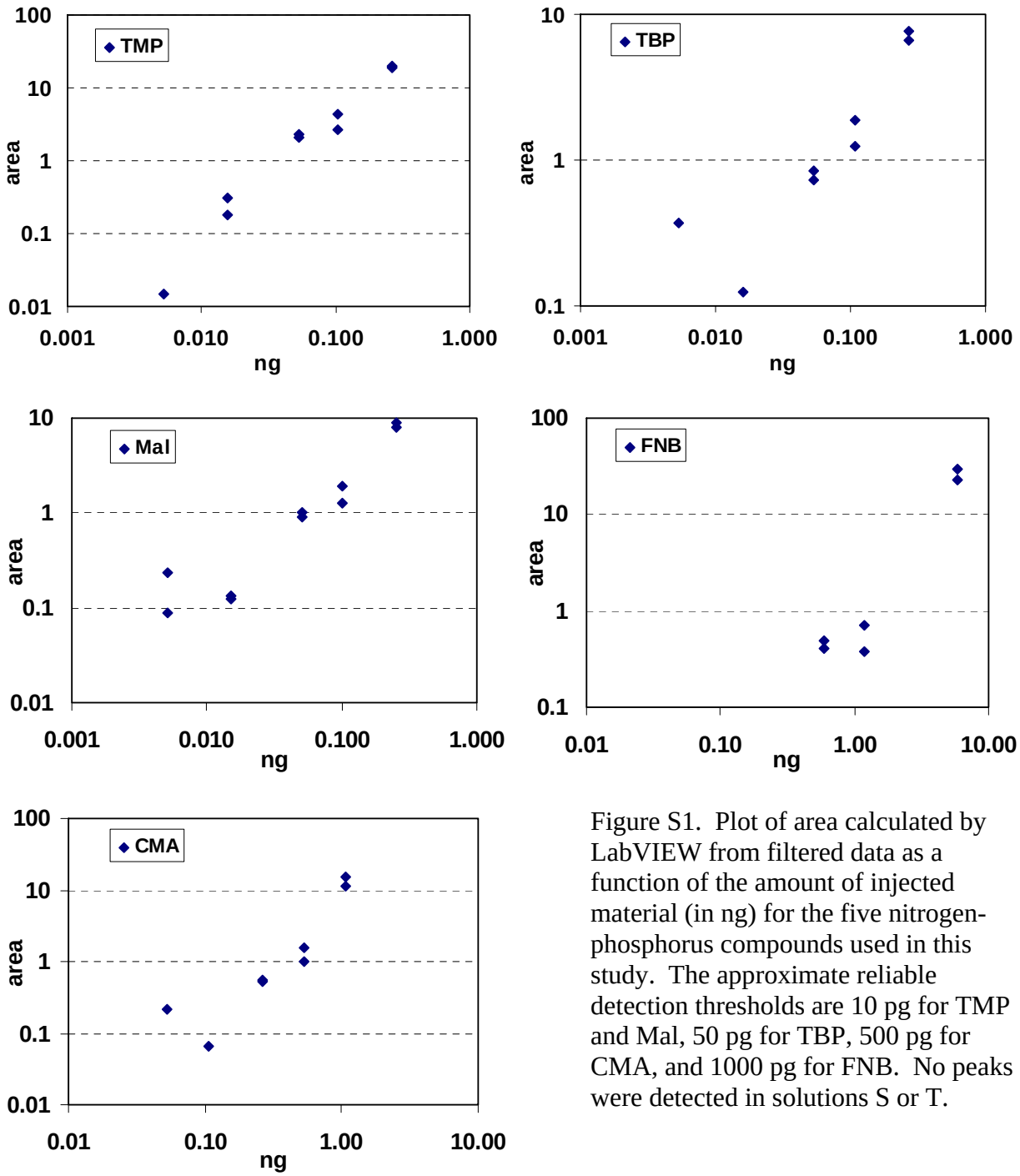

Figure S1. Plot of area calculated by LabVIEW from filtered data as a function of the amount of injected material (in ng) for the five nitrogen-phosphorus compounds used in this study. The approximate reliable detection thresholds are 10 pg for TMP and Mal, 50 pg for TBP, 500 pg for CMA, and 1000 pg for FNB. No peaks were detected in solutions S or T.

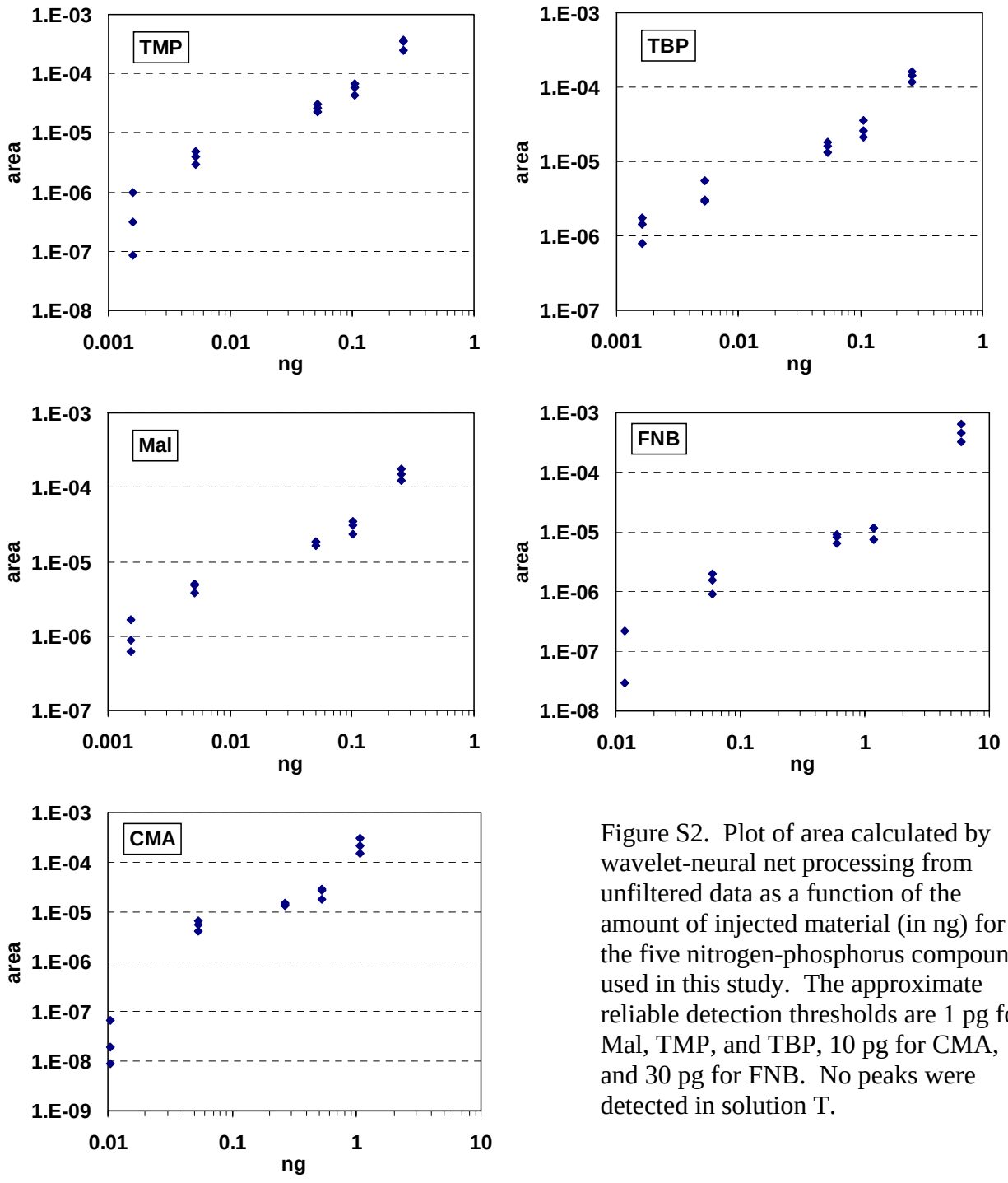

Figure S2. Plot of area calculated by wavelet-neural net processing from unfiltered data as a function of the amount of injected material (in ng) for the five nitrogen-phosphorus compounds used in this study. The approximate reliable detection thresholds are 1 pg for Mal, TMP, and TBP, 10 pg for CMA, and 30 pg for FNB. No peaks were detected in solution T.

During the course of the experiments, certain “extraneous” peaks appeared reproducibly. It was postulated that these were due to impurities in the solvent, since they would be independent of the concentration of spiked compounds. An aliquot of solvent was evaporated 100-fold, and multiple GC runs were made. After wavelet-neural net processing, several peaks did appear reproducibly. Figure S3 shows an overlay of six chromatographs from the concentrated solvent along with a portion of the chromatogram of one of the dilute spiked solutions, also processed by the wavelets and neural networks. Extraneous peaks at 1.27, 1.48, and 1.51 minutes that appear in the spiked solution correlate well with peaks in the concentrated solvent. Another peak at 1.89 min does not appear in this particular sample, either because it was a contaminant not in the original solvent that was picked up during handling or because it was missed by the data reduction. However, all of the “solvent impurity” peaks do show up in trace levels in one of the blind test samples, as shown in Figure S4.

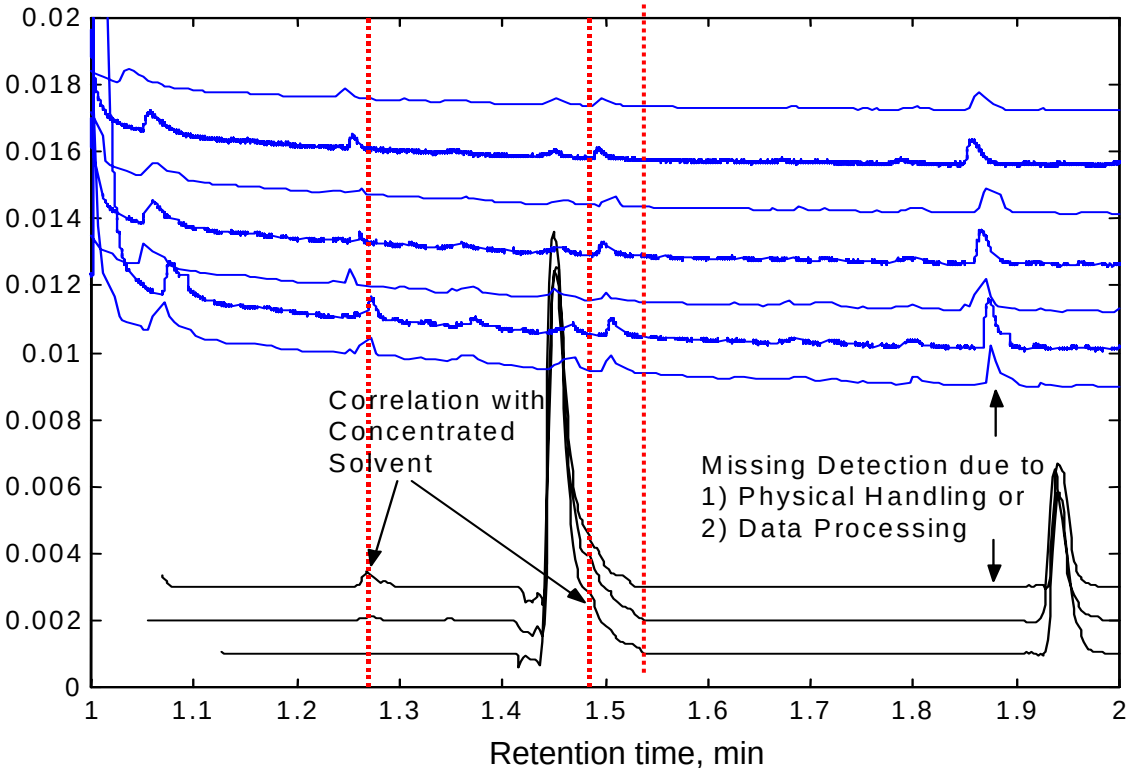

Figure S3. Comparison of minor peaks detected during multiple injections of a solvent concentrate compared to minor peaks detected in one of the dilute calibration solutions.

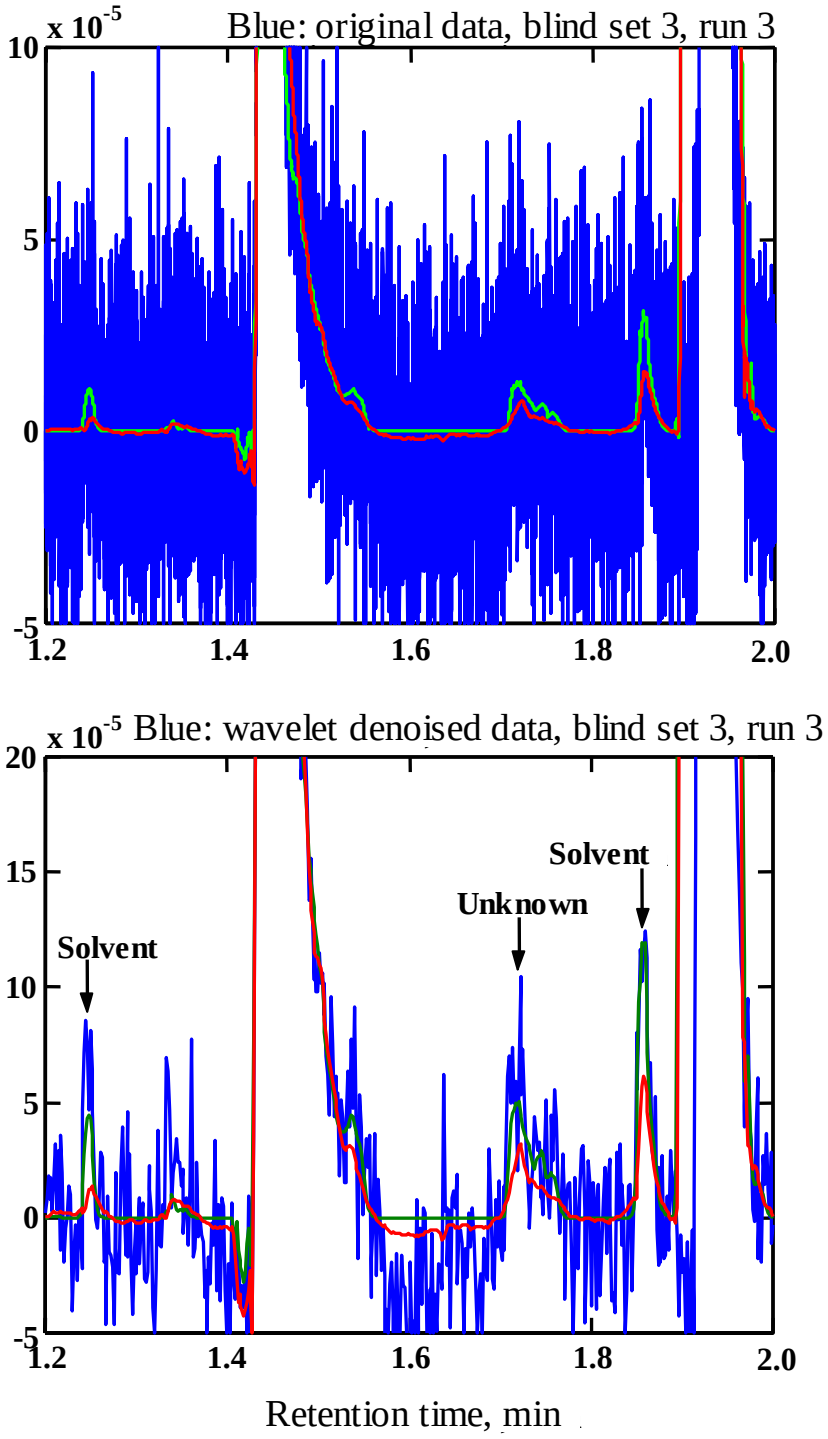

Figure S4. Comparison of wavelet/neural network processed data for one of the blind test solutions with the raw data (top-blue) and the wavelet denoised data (bottom-blue). Note that small peaks at 1.25, 1.55, and 1.87 min correspond to solvent impurities shown in Figure S3. The green and red curves represent results from two different neural networks using the same wavelet preprocessing.